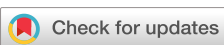


RESEARCH ARTICLE | FEBRUARY 21 2023

Scalable selective absorber with quasiperiodic nanostructure for low-grade solar energy harvesting

Special Collection: Photonic Structures for Efficient Thermal Management

Zifu Xu ; Ying Li ; Gang Gao; Fei Xie; Ran Ju; Shimin Yu; Kaipeng Liu; Jiaxin Li ; Wuyi Wang; Wei Li ; Tianlong Li ; Cheng-Wei Qiu 

APL Photonics 8, 020801 (2023)

<https://doi.org/10.1063/5.0135193>

View Online



Export Citation

CrossMark

Articles You May Be Interested In

Some properties of quasiperiodic subshifts

AIP Conference Proceedings (December 2019)

Quasiperiodic quantum states

J. Chem. Phys. (June 1984)

Experimental investigation of quasiperiodic-chaotic-quasiperiodic-chaotic transition in a direct current magnetron sputtering plasma

Physics of Plasmas (August 2015)

AMERICAN ELEMENTS
THE ADVANCED MATERIALS MANUFACTURER 

sapphire windows	Nd:YAG	yttrium iron garnet	glassy carbon	beamsplitters	fused quartz	additive manufacturing
spintronics	raman substrates	zeolites	III-IV semiconductors	gallium lump	copper nanoparticles	organometallics
silver nanoparticles	perovskites	cerium oxide polishing powder	europium phosphors	photronics	infrared dyes	
MOICVD	beta-barium borate	epitaxial crystal growth	ultra high purity materials	transparent ceramics	CIGS	
rare earth metals	quantum dots	surface functionalized nanoparticles	He	cermet	nanodispersions	
osmium	scintillation Ce:YAG	Al Si P S Cl Ar	He	MBE grade materials	thin film	
refractory metals	laser crystals	Ga As Ge As Se Br Kr	cerium	OLED lighting	solar energy	
anodic aluminum nitobate	InAs wafers	In Sn Sb Te I Xe	ceramic	growing	fiber optics	
perovskite crystals	MOFs	Tl Pb Bi Pb Pb I Al Rh	nanoparticles	targets	h-BN	
	AuNPs	Tl Pb Bi Pb Pb I Al Rh	MBE	deposition slugs	deposition	
	ZnS CdTe	Tl Pb Bi Pb Pb I Al Rh	grade	targets	slugs	
	transparent ceramics	Tl Pb Bi Pb Pb I Al Rh	materials	CDV precursors	photovoltaics	
		Tl Pb Bi Pb Pb I Al Rh	ceramic	metamaterials	h-BN	
		Tl Pb Bi Pb Pb I Al Rh	nanodispersions	borosilicate glass	deposition	
		Tl Pb Bi Pb Pb I Al Rh	MBE	YBCO	slugs	
		Tl Pb Bi Pb Pb I Al Rh	grade	superconductors	metamaterials	
		Tl Pb Bi Pb Pb I Al Rh	ceramic	InGaAs	borosilicate	
		Tl Pb Bi Pb Pb I Al Rh	nanoparticles	indium tin oxide	glass	
		Tl Pb Bi Pb Pb I Al Rh	MBE	MgF ₂	rutile	
		Tl Pb Bi Pb Pb I Al Rh	grade	diamond micropowder	diamond	
		Tl Pb Bi Pb Pb I Al Rh	ceramic	optical glass	micropowder	

The Next Generation of Material Science Catalogs

Now Invent.™

www.americanelements.com
© 2001-2023 American Elements is a U.S. Registered Trademark

Scalable selective absorber with quasiperiodic nanostructure for low-grade solar energy harvesting



Cite as: APL Photon. 8, 020801 (2023); doi: 10.1063/5.0135193

Submitted: 17 November 2022 • Accepted: 16 January 2023 •

Published Online: 21 February 2023



Zifu Xu,^{1,2} Ying Li,^{3,4,a)} Gang Gao,⁵ Fei Xie,⁶ Ran Ju,^{3,4} Shimin Yu,¹ Kaipeng Liu,¹ Jiaxin Li,² Wuyi Wang,¹ Wei Li,^{6,a)} Tianlong Li,^{1,a)} and Cheng-Wei Qiu^{2,a)}

AFFILIATIONS

¹ State Key Laboratory of Robotics and System, Harbin Institute of Technology, Harbin, Heilongjiang 150001, China

² Department of Electrical and Computer Engineering, National University of Singapore, Kent Ridge 117583, Singapore

³ State Key Laboratory of Modern Optical Instrumentation, Interdisciplinary Center for Quantum Information, ZJU-Hangzhou Global Scientific and Technological Innovation Center, Zhejiang University, Hangzhou 310027, China

⁴ Key Laboratory of Advanced Micro/Nano Electronic Devices and Smart Systems of Zhejiang, International Joint Innovation Center, The Electromagnetics Academy of Zhejiang University, Zhejiang University, Haining 314400, China

⁵ National Key Laboratory of Science and Technology on Advanced Composites in Special Environments, Harbin Institute of Technology, Harbin 150080, China

⁶ GPL Photonics Laboratory, State Key Laboratory of Applied Optics, Changchun Institute of Optics, Fine Mechanics and Physics Chinese Academy of Sciences, Changchun 130033, China

Note: This paper is part of the APL Photonics Special Topic on Photonic Structures for Efficient Thermal Management.

a) Authors to whom correspondence should be addressed: eleying@zju.edu.cn; tianlongli@hit.edu.cn; weili@ciomp.ac.cn; and chengwei.qiu@nus.edu.sg

ABSTRACT

Although the solar-thermal technology has opened up a potential green energy harvesting method, it is challenging to suppress the non-negligible energy dissipation while maintaining a high absorbance. Most disordered organic polymers are almost incapable of limiting the absorption in the desired cutoff wavelength range, which is detrimental to the design of selective absorbers. Moreover, the development of absorbers with a periodic plasmonic nanostructure is always lacking in cost-effective scalability. Herein, we report a scalable selective absorber with a quasiperiodic nanostructure composed by an economical widespread surface self-assembly of densely arranged Fe_3O_4 nanoparticles, possessing a high-performance energy conversion for low-grade solar energy. By investigating the scale effect of the quasiperiodic densely arranged plasmonic nanostructure, a significant solar absorption $>94\%$ and ideal passive suppression of thermal emissivity <0.2 can be obtained simultaneously. With the synergy of material properties, thermal management, and environmental effect, a flexible planar solar thermoelectric harvester is demonstrated under natural sunlight (AM1.5G), reaching a significant sustaining open-circuit voltage of $>20 \text{ mV/cm}^2$, without a heat sink. This highly versatile strategy is expected to lead the exploration of energy evolution in fundamental research and pioneer next-generation, high-performance, economical, and practical solar co-harvesting systems.

© 2023 Author(s). All article content, except where otherwise noted, is licensed under a Creative Commons Attribution (CC BY) license (<http://creativecommons.org/licenses/by/4.0/>). <https://doi.org/10.1063/5.0135193>

27 August 2023 14:10:28

I. INTRODUCTION

As the current energy crisis compels humanity to search for alternatives to fossil energy industry,¹ realizing clean and permanent energy harvesting has become a long-standing developing strategy. Solar energy has been considered as one of the most ideal available

resources because of the stability of optical field, enabling broad applications in solar photovoltaic,^{2,3} solar-thermal,^{4,5} and solar-chemical approaches.⁶ Thereinto, the solar-thermal technology with a minimum carbon footprint can convert photons into thermal energy directly, which has been proposed as an efficient

solar-trapping component that can be integrated in solar-thermal structural engineering for desalination^{7–9} and energy generation.^{7,10–12} The most vital demand in the technology is attributable to the efficient net heat accumulation for highly effective solar-thermal conversion under a low solar radiation flux.^{9,13,14} Under this case, a subwavelength plasmonic nanostructure and carbon-based polymeric materials^{10,18,19} have been widely exploited to achieve efficient broadband sunlight absorption and rapid heat relaxation. However, non-negligible heat dissipation always remains in the non-equilibrium thermalization and can even exceed 60% when the blackbody absorber reaches 100 °C.^{14,20,21} Thus, restraining the excessive thermal radiation while maintaining a high absorbance is a critical consideration. To address this drawback, some efforts have focused on periodic plasmonic structures with selective spectral absorption, which is beneficial to limit the absorption in the desired cutoff wavelength range compared to most disordered organic polymers^{8,22,23} and has been gradually explored for solar vapor generation and water heating with commerciality.^{24,25} Nevertheless, the advanced strategies with a direct spectral selectivity are always restricted by unscalable costly nano-engineering,^{9,23,26} which limits the future widespread application. Therefore, developing a highly versatile strategy for theoretically guiding designs of selective solar-thermal devices and economical large-scale popularization is of great significance in fundamental research and industrial implementation.

Herein, we propose a selective absorber with a quasiperiodic nanostructure for scalable solar-thermal engineering, which is verified to have a significant solar absorption and passive suppression of thermal radiation, possessing an ideal solar-thermal conversion. We investigate the hybrid interactions in the nanostructure and the energy evolution during the non-equilibrium thermalization, finding that the far-field thermal radiation can be suppressed by the arranged density of the plasmonic nanostructure due to near-field in-phase interactions and negative-temperature-correlativity, which induces a selective spectral absorption in the quasiperiodic nanostructure. By abandoning the cumbersome and costly nano-fabrication, the scalable solar absorber can be fabricated via the cost-effective surface self-assembly of quasiperiodic densely

arranged Fe_3O_4 nano-particles, with a high absorbance of >94% and passive suppression of thermal emissivity of <0.2. For practicality, by synergizing material properties, thermal management, and environmental effect, a flexible planar solar thermoelectric harvester is demonstrated under natural sunlight (AM1.5G), reaching a sustaining open-circuit output of >20 mV/cm². At lower ambient temperatures, the performance can be prominently increased, over 20%.

II. RESULTS AND DISCUSSION

In nature, as a low-grade heat source, solar radiation density absorption localizes mainly from ultraviolet (UV) to near-infrared (NIR). The solar-thermal devices always emit energy by lossy thermal radiation across mid-IR range²⁷ (MIR, 8–14 μm) to atmosphere while obtaining solar energy across UV-NIR [shown in Fig. 1(a)]. The efficiency²⁸ of solar-thermal η_{OT} is always affected by solar absorbance and thermal losses during the thermalization as $\eta_{OT} = \frac{I}{I_{solar}} = \frac{\int d\lambda \alpha_{(\lambda)} I_{(\lambda)}}{\int d\lambda I_{(\lambda)}} - \varepsilon_{eff}(T) \int_{\lambda_1}^{\lambda_2} I_b(\lambda, T) d\lambda$. Here, $\alpha_{(\lambda)}$ and $I_{(\lambda)}$ represent the monochromatic absorbance of solar absorbers and the monochromatic solar radiation intensity, respectively, $\varepsilon_{eff}(T)$ is the equivalent thermal emissivity of the absorbers, and $\int_{\lambda_1}^{\lambda_2} I_b(\lambda, T) d\lambda \approx \sigma(T_{amb} + \Delta T)^4$ depicts the radiative intensity of a blackbody. As the solar thermal conversion reaches equilibrium state, I_{solar} is constant. The temperature-rise of solar-thermal devices ΔT is written as

$$\Delta T = \sqrt[4]{\frac{\int d\lambda \alpha_{(\lambda)} I_{(\lambda)} / I_{solar}}{\varepsilon_{eff}(T)} - T_{amb}} \quad (1)$$

As one can see from Eq. (1), the high absorbance and low emissivity can increase the values of ΔT . Therefore, a significant temperature rise can be generated quickly by a solar absorber with significant selective absorption and low thermal emissivity, which can provide the possibility to enhance the practicality of solar energy harvesting. Meanwhile, a decline in the ambient temperature T_{amb}

27 August 2023 14:10:28

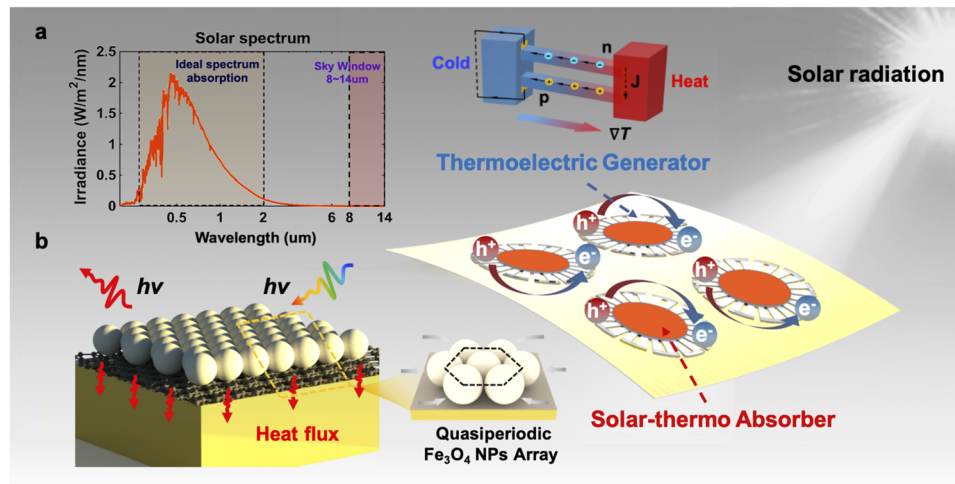


FIG. 1. Solar-thermal conversion and solar thermoelectric harvesting from low-grade solar energy via the quasiperiodic scalable selective solar absorber. (a) Ideal spectral solar absorption localizes mainly between 0.3 and 2 μm, ranging from ultraviolet to near-infrared. The pink block represents the atmospheric window across 8–14 μm for main thermal radiation of the absorber. (b) Schematic of the solar-thermal conversion via the quasiperiodic selective solar absorber. The right inset displays a flexible planar solar thermoelectric harvester for low-grade solar energy based on solar-heat-driven Seebeck effect.

can also increase the solar-thermal performance, which is beneficial for application in cool outdoor environments. In this work, we proposed a selective absorber composed of densely arranged Fe_3O_4 nano-particles coated on the graphite–metal substrate, as illustrated in Fig. 1(b). The nanostructure is patterned in a quasi-C6-symmetry and possesses a superior structural stability in 2D configuration, whose natural quasiperiodic structure provides the possibility of scalable selective solar-thermal conversion. Based on the highly versatile strategy, we promote a scalable guideline for exploring a photon–heat–electron conversion by integrating a flexible planar solar thermoelectric harvester for low-grade solar energy, which is expected to provide a platform for the next-generation, high-performance, economical, and practical solar co-harvesting systems.

Under the weak electromagnetic force, the value of the equilibrium separation of nano-particles fluctuates around the particle diameter. Therefore, the group of plasmonic nanostructure can approximate the face-centered cubic lattice with structural stability at mesoscopic scale.²⁹ Dependent on the reduction in periodicity, we approximated an equivalent lattice-spacing C6 rotational symmetric unit-cell including six coupled adjacent and one central plasmonic nanostructure. When the nanostructure is excited with optical illumination, forward scattering is usually enhanced in the Mie-mode, which induces a strong plasmonic resonance.^{30,31} In a non-Hermitian system, the non-equilibrium thermalization drives ultrafast heat evolution for heating up along with thermal radiation. As shown in Fig. 2(a), the adjacent plasmonic

nanostructure in the same phase couples in near-field region and modulate far-field thermal emission around the resonant frequency. As described in quasinormal mode theory,³² the reduced radiation flux from nano-resonators is the sum of the contributions from thermal emissions at multiple resonant modes.³³ According to the hybrid nanostructure in this work, the normalized thermally excited radiation spectra to far-field at multiple predominant resonant modes from a single nanostructure is plotted in Fig. 2(b). Multiple narrow-band peaks appear in the visible regime, which indicates that the hybrid nanostructure has broadband radiation/absorption based on Kirchhoff's law. In contrast, a single predominant resonant mode appears in the MIR regime, which benefits the modulation of the far-field thermal radiation.

First, we investigated the optical absorption of the densely arranged plasmonic nanostructure in visible regime, which is preset to separate a distance of 30 nm. In the visible regime, the electric field is nearly bounded around a graphite layer and Fe_3O_4 nano-particles and generates sharp thermalization for increasing the temperature of the absorber [Figs. S2.1(a) and S2.1(b)]. To maximize the energy absorption in terms of energy balanced equation, a genetic algorithm is adopted to optimize the parameters of graphite layer thickness and particle size. Considering the preparation process of Fe_3O_4 nano-particles and graphite layer, the particle radius and layer thickness are difficult to be over the limits, 280 and 50 nm, respectively. In this case, the optimized particle size and the graphite layer thickness are $r = 260 \text{ nm}$ and $d = 45 \text{ nm}$, respectively, where the solar absorption efficiency can be raised to 96.5%, as shown in Fig. 2(c).

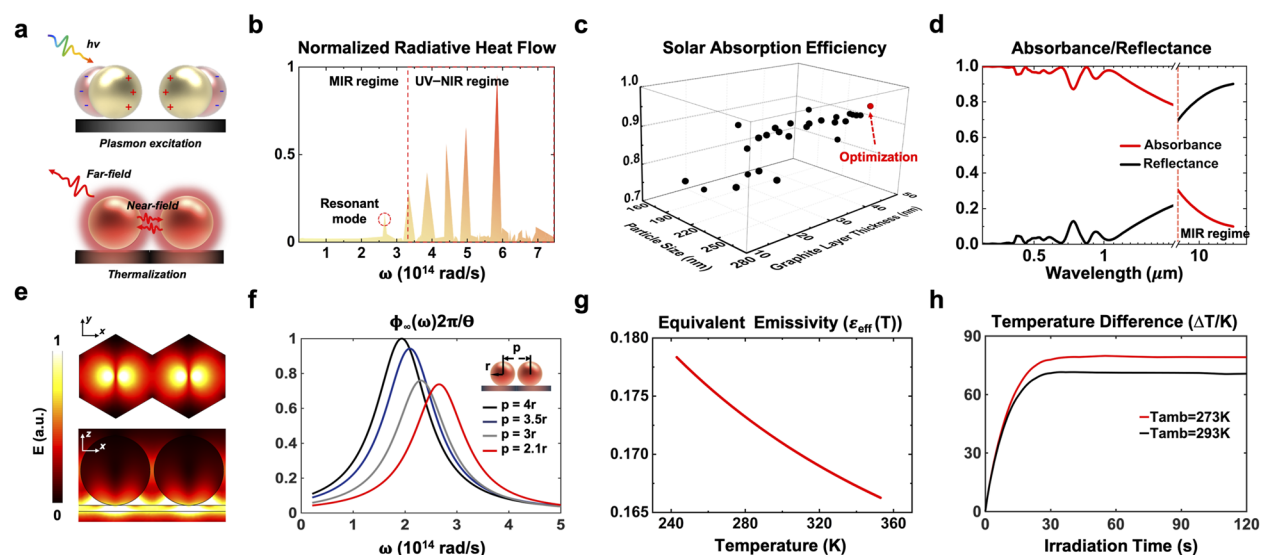


FIG. 2. Solar-thermal conversion performances of the selective absorber. (a) Schematic of plasmonic excitation and non-equilibrium thermalization of the plasmonic nanostructure array. (b) Normalized thermal radiative heat flow from a single plasmonic nanostructure inside the densely arranged array. (c) Optimized plasmonic nanostructure via genetic algorithm, characterized by the structural parameters: the radius of the Fe_3O_4 nano-particle and the thickness of the graphite layer. (d) Simulated absorbance and reflectance of the solar absorber (across UV-NIR spectrum $0.3\text{--}2 \mu\text{m}$ and MIR regime $8\text{--}14 \mu\text{m}$). (e) Electric field profiles of the predominant resonant mode of two densely arranged adjacent plasmonic nanostructures in the MIR regime. (f) Spectral energy flux of far-field thermal emission varied with the arranged density of the plasmonic nanostructure. (g) Modeled equivalent far-field emissivity for the densely arranged plasmonic nanostructure at $8\text{--}14 \mu\text{m}$ across temperatures from 243 to 353 K, which is normalized to blackbody radiation. (h) Time evolution of average temperature rise ($\Delta T = T - T_{\text{amb}}$) of the absorber at a low temperature ($T_{\text{amb}} = 273 \text{ K}$) and room temperature ($T_{\text{amb}} = 293 \text{ K}$), respectively.

Furthermore, Fig. 2(d) simulates the average absorbance spectra across UV–NIR spectrum 0.3–2 μm and MIR regime 8–14 μm , respectively. The absorbance of different polarized light both maintains high efficiency in the UV–NIR regime and low efficiency in the MIR regime, which indicates that the absorber can obtain selective spectral absorbance. In addition, compared to scattered optical energy, over 94% energy can be converted to Ohmic losses inside the plasmonic nanostructure, beneficial for local heating and solar-thermal conversion [Fig. S2.1(d)].

As for the lossy thermal radiation of the absorber, coupled near-field interactions between the adjacent plasmonic nanostructures inside the periodic array become a major factor. By means of the predominant resonant mode in the infrared range in Fig. 2(e), we calculated the spectral energy flux of far-field thermal emission varying with the arranged density of the plasmonic nanostructure in Fig. 2(f) (for details, see the [supplementary material S1](#)). As one can see, the intensity of far-field thermal emission can be negatively correlated with the arranged density of the nano-particles by means of the enhanced coupled near-field interaction. The scale effect of the plasmonic nanostructure not only weakens the narrow band thermal emission at the predominant resonant frequency but also induces the departure of the resonant mode from the atmospheric window. Furthermore, the absorber often stably operates below 100 °C under one sunlight illumination and the emission spectrum is mainly located in the MIR regime, which overlaps the atmospheric window region (8–14 μm). According to Wien's law, the thermal emission spectrum of the blackbody will blueshift to that of the densely arranged plasmonic nanostructure as the temperature rises; therefore, the far-field equivalent thermal emissivity will be weakened reversely, following³⁴

$$\varepsilon_{(\omega,T)} = \frac{\phi_\infty}{\phi_{BB}}. \quad (2)$$

Therefore, we could calculate the equivalent thermal emissivity (8–14 μm) of the absorber under varying temperatures, as shown in Fig. 2(g). One can see that the equivalent far-field thermal emissivity declines with an increase in the heating temperature and maintains below 0.2, which displays the ideal passive suppression of thermal radiation. Furthermore, we calculated the temperature rise and total solar-thermal efficiency with varying ambient temperatures in Figs. S2.2(b) and S2.2(c), and the time-evolution of the average temperature rise with a low temperature (273 K) and room temperature (293 K) is plotted in Fig. 2(h). The selective absorber can sustain a high thermal response before the thermal equilibrium, and the average temperatures rise rapidly to the steady state at \sim 120 s, which indicates the fast thermalization of the plasmonic nanostructure under illumination. In the lower ambient temperature 273 K, the absorber can generate a higher temperature rise of $\Delta T_H \approx 80$ K, compared to that in the room temperature 293 K ($\Delta T_H \approx 70$ K). As a result, the absorber features fast thermalization performance and significant temperature rise under natural solar illumination and displays low-temperature enhanced conversion performance.

For demonstration, we developed a scalable fabrication of the selective hybrid solar absorber [Fig. 3(a)]. The absorber was fabricated via the formation of graphite–copper substrate and the self-assembly of the monolayer Fe_3O_4 nano-particles film, by means of a simple thermal evaporation and the Langmuir–Blodgett technique.^{35,36} Figure 3(b) shows the photograph of the samples and SEM images of the surface of the absorber. The Fe_3O_4 nano-particles are mostly self-patterned in the densely arranged

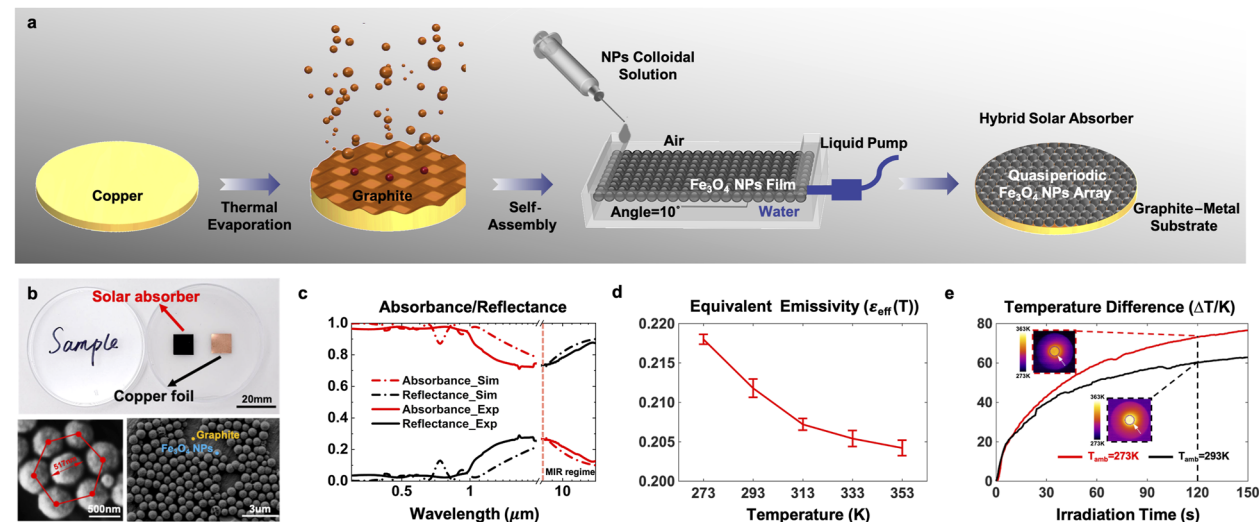


FIG. 3. Fabrication and solar-thermal conversion characterization of the scalable selective solar absorber with quasiperiodicity. (a) Schematic of the steps in the scalable fabrication of the selective solar absorber. (b) Photographs of the solar absorber and copper foil (top), and top-view SEM images of the absorber (bottom). (c) Measured absorbance (red dashed line) and reflectance (black dashed line) spectrum of the absorber. The red line and the black line are the simulated absorbance and reflectance spectrum of the absorber, respectively. (d) Corresponding equivalent far-field emissivities of the solar absorber in the MIR regime (8–14 μm) across temperatures from 273 to 353 K. (e) Temperature rise of the solar absorber after various periods of illumination under ambient temperatures $T_{\text{amb}}=273$ K (red) and $T_{\text{amb}}=293$ K (black). The infrared images show the temperature maps of the solar absorber under one sun illumination after 120 s.

structure (quasi-C6-symmetry), coating the graphite–copper substrate. Figure 3(c) displays the experimental absorbance spectrum, which has a good agreement with the simulated results, especially in the visible light region. The selective solar absorber approaches an efficient absorbance of >94%, which demonstrates a high-efficiency solar-thermal conversion. In contrast, the significantly reduced absorption in the MIR regime shows the selective spectral absorption performance. Although the unflatness of the commercial substrate causes quasiperiodicity of Fe_3O_4 nano-particles array, the absorber still maintains an excellent solar absorption capacity, making it a cost-effective attraction. As for thermal radiation, we focused on the equivalent emissivity of the solar absorber in MIR range (8–14 μm). The experimental results of the equivalent emissivity (8–14 μm) are shown in Fig. 3(d). The equivalent emissivity declines gradually as the temperature increases and always maintains an extremely low value of ~0.2 at the steady-state working temperature, which approximates the theoretical analysis. Figure 3(e) presents the solar-thermal performance of the selective absorber under the solar simulator illumination (AM1.5G). After 120 s of illumination, the temperature rise of the sample increases to ~60 °C in

the room temperature (293 K) environment ($T = 80^\circ\text{C}$). In contrast, the temperature rise of the absorber increases significantly to ~73 °C in a lower temperature (273 K) environment ($T = 73^\circ\text{C}$). The results demonstrate that the absorber possesses an ideal selective solar absorption and a superior low-temperature enhanced solar-thermal conversion performance under one sunlight illumination. In the future, the preparation of substrates with a flatter surface is expected to further improve the quality and performance of the absorber by means of more precise methods, such as electrochemical technology.

Due to the planar thermalization, the strategy possesses promising advantages to develop a flexible energy harvester for low-grade solar energy. Figure 4(a) illustrates a flexible planar solar thermoelectric harvester integrated by the selective absorber and an in-plane thermoelectric chip. The simple pattern-cascaded configuration supports the scalable fabrication through a single- or multi-layer circuit package and possesses a lower electronic cost. Dependent on the remarkable temperature rise of the absorber, a more significant thermoelectromotive force can be generated according to the supplementary material Eq. (14). In particular,

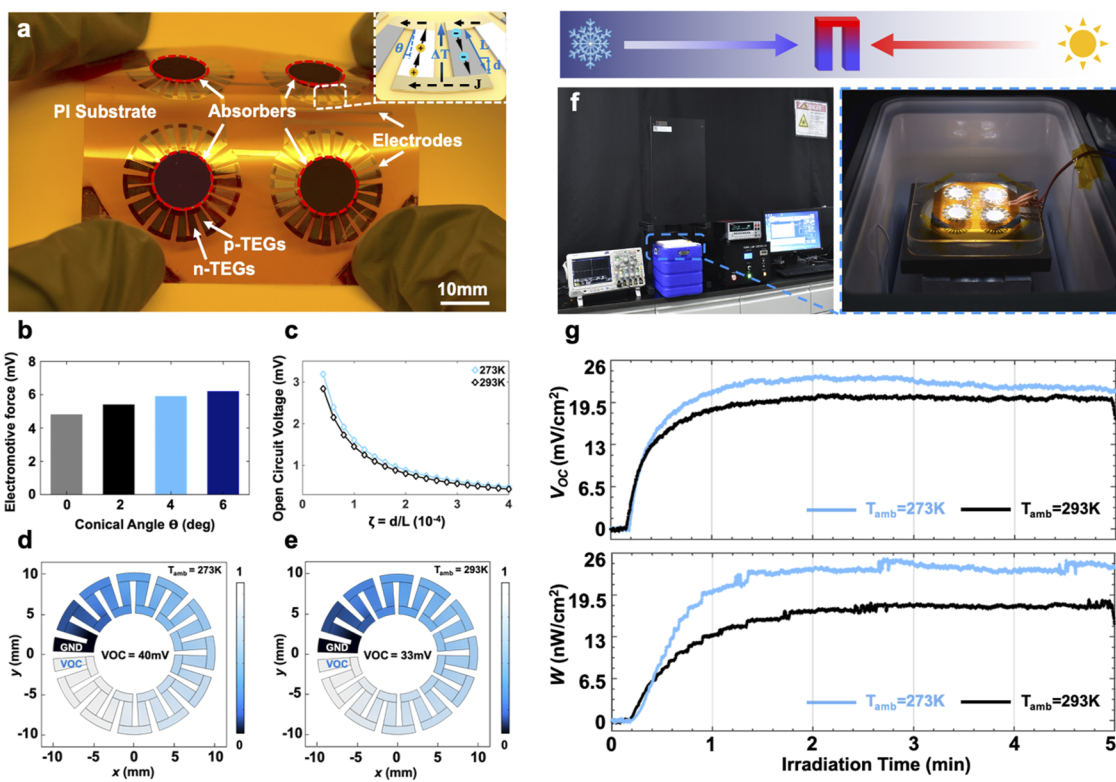


FIG. 4. Low-grade solar energy harvesting via the flexible planar solar thermoelectric harvester. (a) Optical image of the flexible planar solar thermoelectric harvester. (b) The angle-relevant electromotive force across a conical thermoelectric configuration. (c) The open circuit voltage V_{oc} across the thermoelectric leg as the height-length ratio changes at different ambient temperatures (273 and 293 K). (d) and (e) Simulations of stable V_{oc} distribution of the pattern-cascaded thermoelectric generator at a low-temperature (273 K) and room temperature (293 K), respectively. (f) Optical images of the natural sunlight harvesting test. The device is illuminated (under one solar illumination) by a solar simulator and connected in series with an oscilloscope, holding an ambient temperature in an incubator. (g) Total series open-circuit voltage per unit illuminated area V_{oc} (top) and the overall output power per unit illuminated area W (bottom) of the solar harvester under one sun illumination. The black line and the blue line are the performances of the solar thermoelectric harvester in the room temperature and low-temperature environments, respectively.

the thermoelectric configuration and the inner parasitic heat flow are considered in the design to improve the thermoelectric conversion performance. As shown in Figs. 4(b) and 4(c), we calculated the effect of conical angle θ and height-length ratio ξ on the thermoelectric conversion performance by modeling thermoelectric transport under spatial transformation, respectively (for details, see the [supplementary material S4](#)). As one can see, the in-plane conical thermoelectric configuration could achieve structural scalability and internal constrictive resistance, enabling a more significant thermoelectromotive force across a compact structure. The average V_{oc} values curve of a 12-np-pair pattern-cascaded thermoelectric chip is simulated in Fig. S4(e). After a period of 45 s approximately, the stable open-circuit voltage (V_{oc}) distributions at 273 and 293 K in a heat open boundary condition are shown in Figs. 4(d) and 4(e), where the device demonstrates a superior V_{oc} (33 mV) in the room-temperature and (40 mV) in a low-temperature, respectively. The harvesting performances of the flexible planar solar thermoelectric harvester were characterized by using the measurement system shown in Fig. 4(f). We simulated one solar illumination and tested the currents and voltages across the output electrodes under two practical cases: a low-temperature environment and a room-temperature environment (273 and 293 K, respectively), which were simulated by an incubator (the two cases can be maintained for long periods). As shown in Fig. 4(g), the open-circuit voltage per unit illuminated area V_{oc} raises quickly after 1 min illumination without a heat sink, reaching 20 mV/cm² at T = 293 K and 24 mV/cm² at T = 273 K respectively. Moreover, the overall output power per unit illuminated area W of the solar thermoelectric harvester was calculated by multiplying the voltage and the current. The W increased to ~18 nW/cm² at the room temperature (293 K) and ~24 nW/cm² at a lower temperature (273 K) without a load, respectively, which demonstrates enhanced harvesting at a lower-temperature environment, over 20%. In more general practical applications, we believe that a higher efficiency output will be achieved by impedance matching.

It should be acknowledged that a restriction of heat exchange and thermoelectric conversion is non-negligible between the solar absorber and the thermoelectric chip, which could be solved by developing an insulating package with a better heat transfer in the future. Nevertheless, the design concept of the solar-heat-driven thermoelectric harvester still demonstrates a remarkable low-grade solar energy harvesting, opening up a promising strategy for scalable applications in the field of photovoltaic-thermoelectric solar co-harvesting.

III. CONCLUSIONS

In this work, we develop a quasiperiodic scalable selective absorber with high-performance solar-thermal conversion for low-grade solar energy. Due to the scale effect of the densely arranged plasmonic nanostructure, the intensity of far-field thermal emission can be suppressed, which addresses the ideal selective spectral absorption and negative-temperature-correlated thermal radiation. By abandoning the cumbersome and costly nano-fabrication, a selective hybrid solar absorber is fabricated by the economical widespread surface self-assembly of quasiperiodic densely arranged Fe₃O₄ nano-particles on the graphite-metal substrate, leading to a significant solar absorbance of >94% and passive suppression of

thermal emissivity of <0.2. By means of the strategy, a flexible planar solar thermoelectric harvester is fabricated for natural sunlight, demonstrating a sustaining open-circuit voltage of >20 mV/cm² under AM1.5G, without a heat sink. This highly versatile strategy offers a promising opportunity to explore energy evolution in fundamental research and industrial implementation and encourages future development in the next-generation widespread solar co-harvesting architecture.

IV. MATERIAL AND METHODS

A. Quasiperiodic scalable selective absorber fabrication and characterization

The proposed selective solar absorber was prepared by a two-step process: the fabrication of the graphite–copper substrate and the monolayer self-assembly of Fe₃O₄ nanoparticles. Pieces of 50 μ m copper foil were first treated with dilute hydrochloric acid to remove the oxidation film and cleaned in acetone and deionized water. For enhancing the interface bonding of graphite–copper layers, the top surface of copper was modified in a plasma cleaner. After that, a 45 nm thin-film of graphite was deposited on the copper foil by a thermal evaporator. Methanol (Aladdin) was then used to modify the graphite layer's hydrophilic property. Next, the Fe₃O₄ NPs (Aladdin) were separated via washing and centrifugal separation. Methanol and chloroform were added at 1:1, to prepare a colloidal dispersion, followed by 3 min ultrasonic dispersion. The self-assembly of Fe₃O₄ NPs can be performed via the Langmuir–Blodgett film deposition technique, carrying out the formation of the surface particle film and ensuring the homogeneity of the monolayer, at the air/water interface. The obtained graphite–copper substrate was placed below the liquid level at 10° angle, pumping the base liquid and vertically lifting slowly for NPs deposition, with a large number of Fe₃O₄ NPs self-assembled in a C6 pattern coated on the substrate.

Top-view profiles of the absorber samples were observed using a field emission SEM (Thermofisher, Scios 2). The spectral reflectance (0.3–2 and 8–14 μ m) of the sample was measured using a UV–visible–NIR spectrophotometer (Shimadzu, UV-3600Plus) with an integrating sphere. The absorption (A) was calculated from the measured reflectance (R) using the equation A = 1 – R. The temperature-varying efficient thermal emission of the samples over 8–14 μ m was measured by an IR hemispherical emissometer. To demonstrate the solar-thermal performance, a solar simulator with an AM1.5G filter is used as the light source (SanYou, SS-50), with an incident flux measurement by a calibrated power meter. The temperature data were collected with a chip thermal sensor (OMRON).

B. Flexible planar solar thermoelectric harvester fabrication and characterization

The thermoelectric generators (inner diameter: 5 mm; external diameter: 10 mm) were deposited on a flexible polyimide substrate (75 μ m) by a thermal evaporator. The polyimide-substrate was cleaned thoroughly by acetone and deionized water for 10 min in an ultrasonic bath. In order to maximize the thermoelectromotive force, the thermoelectric element cross-sectional area ratio has to be matched to the material properties.³⁷ Herein, the conical angle

ratio can become $\frac{\theta_n}{\theta_p} = \frac{A_n}{A_p} = \sqrt{\frac{\sigma_p K_p}{\sigma_n K_n}}$, with 9° for the p-type material and 10° for the n-type material. The target materials of p-type and n-type for evaporation were $\text{Bi}_{0.5}\text{Sb}_{1.5}\text{Te}_3$ and $\text{Bi}_2\text{Te}_{2.7}\text{Se}_{0.3}$, respectively, and were coated on the PI-substrate for 3 h, which can be connected in a series circuit by Au thin-film electrodes deposited by a thermal evaporator using Au target (99.999%). The thermoelectric capabilities of the thermoelectric generators (conductivity, Seebeck coefficient, and power factor) were measured by a ZEM3 system (ULVAC) (see the [supplementary material](#) Table).

The solar absorber was integrated with the thermoelectric generators for the flexible planar solar thermoelectric harvester in the same plane by silicone grease. The solar simulator with an AM1.5G filter was used as the light source for demonstrating the natural sunlight harvesting (SanYou, SS-50). We simulated two cases for a low-temperature environment and room-temperature environment (273 and 293 K) by an incubator and simultaneously measured both the current and the V_{oc} across the electrodes at the output port of the solar thermoelectric harvester. The overall output power of the solar thermoelectric harvesting was calculated by multiplying the voltage and the current.

SUPPLEMENTARY MATERIAL

See [supplementary material](#) for the complete solar-thermal conversion performance and thermoelectric application of the studied absorber.

ACKNOWLEDGMENTS

Y.L. acknowledges the support from Key Research and Development Program of the Ministry of Science and Technology (Grant No. 2022YFA1405200), the National Natural Science Foundation of China (Grant Nos. 92163123 and 52250191), and the Fundamental Research Funds for the Central Universities (Grant No. 2021FZZX001-19). C.-W.Q. acknowledges financial support from the Ministry of Education, Singapore (Grant No. A-0005143-01-00). T.L. acknowledges the support from the National Natural Science Foundation of China (Grant No. 52175009), Natural Science Foundation of Chongqing (Grant No. CSTB2022NSCQ-MSX0507), Natural Science Foundation of Heilongjiang Province (Grant No. YQ2022E022), and Fundamental Research Funds for Central Universities. W.L. acknowledges the support from the National Natural Science Foundation of China (Grant Nos. 62134009 and 62121005). Z.X. acknowledges the China Scholarship Council (CSC) for financial support.

AUTHOR DECLARATIONS

Conflict of Interest

The authors have no conflicts to disclose.

Author Contributions

Z.X. and Y.L. contributed equally to this work.

Zifuxu: Data curation (equal); Investigation (lead); Software (lead); Validation (lead); Visualization (lead); Writing – original draft

(lead). **Ying Li**: Conceptualization (equal); Funding acquisition (equal); Project administration (lead); Resources (equal); Supervision (equal); Writing – original draft (supporting); Writing – review & editing (lead). **Gang Gao**: Investigation (supporting); Resources (equal); Validation (supporting). **Fei Xie**: Data curation (supporting); Investigation (supporting); Resources (supporting). **Ran Ju**: Investigation (supporting); Software (supporting); Validation (supporting). **Shimin Yu**: Data curation (supporting); Investigation (supporting); Resources (supporting). **Kaipeng Liu**: Investigation (supporting); Software (supporting). **Jiaxin Li**: Investigation (supporting); Software (supporting). **Wuyi Wang**: Formal analysis (supporting); Supervision (supporting). **Wei Li**: Conceptualization (supporting); Funding acquisition (equal); Methodology (supporting); Resources (supporting); Writing – review & editing (supporting). **Tianlong Li**: Funding acquisition (equal); Project administration (equal); Supervision (equal); Writing – review & editing (supporting). **Cheng-Wei Qiu**: Conceptualization (equal); Formal analysis (equal); Project administration (supporting); Writing – review & editing (equal).

DATA AVAILABILITY

The data that support the findings of this study are available from the corresponding authors upon reasonable request.

REFERENCES

- ¹K. Barnham, K. Knorr, and M. Mazzer, “Progress towards an all-renewable electricity supply,” *Nat. Mater.* **11**, 908 (2012).
- ²R. R. Hernandez, A. Armstrong, J. Burney, G. Ryan, K. Moore-O’Leary, I. Diédiou, S. M. Grodsky, L. Saul-Gershenson, R. Davis, J. Macknick, D. Mulvaney, G. A. Heath, S. B. Easter, M. K. Hoffacker, M. F. Allen, and D. M. Kammen, “Techno-ecological synergies of solar energy for global sustainability,” *Nat. Sustainability* **2**, 560 (2019).
- ³A. Polman, M. Knight, E. C. Garnett, B. Ehrler, and W. C. Sinke, “Photovoltaic materials: Present efficiencies and future challenges,” *Science* **352**, aad4424 (2016).
- ⁴G. Baffou, F. Cichos, and R. Quidant, “Applications and challenges of thermoplasmonics,” *Nat. Mater.* **19**, 946 (2020).
- ⁵P. Tao, G. Ni, C. Song, W. Shang, J. Wu, J. Zhu, G. Chen, and T. Deng, “Solar-driven interfacial evaporation,” *Nat. Energy* **3**, 1031 (2018).
- ⁶T. Banerjee, F. Podjaski, J. Kröger, B. P. Biswal, and B. V. Lotsch, “Polymer photocatalysts for solar-to-chemical energy conversion,” *Nat. Rev. Mater.* **6**, 168 (2021).
- ⁷M. Gao, L. Zhu, C. K. Peh, and G. W. Ho, “Solar absorber material and system designs for photothermal water vaporization towards clean water and energy production,” *Energy Environ. Sci.* **12**, 841 (2019).
- ⁸L. Zhou, Y. Tan, J. Wang, W. Xu, Y. Yuan, W. Cai, S. Zhu, and J. Zhu, “3D self-assembly of aluminium nanoparticles for plasmon-enhanced solar desalination,” *Nat. Photonics* **10**, 393 (2016).
- ⁹K. T. Lin, H. Lin, T. Yang, and B. Jia, “Structured graphene metamaterial selective absorbers for high efficiency and omnidirectional solar thermal energy conversion,” *Nat. Commun.* **11**, 1389 (2020).
- ¹⁰L. Zhu, T. Ding, M. Gao, C. K. N. Peh, and G. W. Ho, “Shape conformal and thermal insulative organic solar absorber sponge for photothermal water evaporation and thermoelectric power generation,” *Adv. Energy Mater.* **9**, 1900250 (2019).
- ¹¹Q. Zhao, A. Huang, X. Ai, J. Liao, Q. Song, H. Reith, X. Cao, Y. Fang, G. Schierning, K. Nielsch, S. Bai, and L. Chen, “Transparent power-generating windows based on solar-thermal-electric conversion,” *Adv. Energy Mater.* **11**, 2101213 (2021).

- ¹²S. Yang, Y. Zhang, J. Bai, Y. He, X. Zhao, and J. Zhang, “Integrating dual-interfacial liquid metal based nanodroplet architectures and micro-nanostructured engineering for high efficiency solar energy harvesting,” *ACS Nano* **16**, 15086 (2022).
- ¹³Q. Liao, P. Zhang, H. Yao, H. Cheng, C. Li, and L. Qu, “Reduced graphene oxide-based spectrally selective absorber with an extremely low thermal emittance and high solar absorptance,” *Adv. Sci.* **7**, 1903125 (2020).
- ¹⁴Y. Li, C. Lin, Z. Wu, Z. Chen, C. Chi, F. Cao, D. Mei, H. Yan, C. Y. Tso, C. Y. H. Chao, and B. Huang, “Solution-processed all-ceramic plasmonic metamaterials for efficient solar-thermal conversion over 100–727 °C,” *Adv. Mater.* **33**, 2005074 (2021).
- ¹⁵S. Kim, J.-M. Kim, J.-E. Park, and J.-M. Nam, “Non noble-metal-based plasmonic nanomaterials: Recent advances and future perspectives,” *Adv. Mater.* **30**, 1704528 (2018).
- ¹⁶W. Ali, M. F. Mideksa, K. Hou, H. Li, X. Wang, and Z. Tang, “All-solution-processed ultrahigh broadband and wide-angle perfect absorber based on Mxene–gold nanoparticles,” *Adv. Opt. Mater.* **8**, 2000447 (2020).
- ¹⁷T. Ding, Y. Zhou, W. L. Ong, and G. W. Ho, “Hybrid solar-driven interfacial evaporation systems: Beyond water production towards high solar energy utilization,” *Mater. Today* **42**, 178 (2021).
- ¹⁸H. Ghasemi, G. Ni, A. M. Marconnet, J. Loomis, S. Yerci, N. Miljkovic, and G. Chen, “Solar steam generation by heat localization,” *Nat. Commun.* **5**, 4449 (2014).
- ¹⁹Z. Yu, S. Cheng, C. Li, L. Li, and J. Yang, “Highly efficient solar vapor generator enabled by a 3D hierarchical structure constructed with hydrophilic carbon felt for desalination and wastewater treatment,” *ACS Appl. Mater. Interfaces* **11**, 32038 (2019).
- ²⁰G. Ni, G. Li, S. V. Boriskina, H. Li, W. Yang, T. Zhang, and G. Chen, “Steam generation under one sun enabled by a floating structure with thermal concentration,” *Nat. Energy* **1**, 16126 (2016).
- ²¹Y. Li, W. Li, T. Han, X. Zheng, J. Li, B. Li, S. Fan, and C.-W. Qiu, “Transforming heat transfer with thermal metamaterials and devices,” *Nat. Rev. Mater.* **6**, 488 (2021).
- ²²Y. Hu, H. Ma, M. Wu, T. Lin, H. Yao, F. Liu, H. Cheng, and L. Qu, “A reconfigurable and magnetically responsive assembly for dynamic solar steam generation,” *Nat. Commun.* **13**, 4335 (2022).
- ²³I. E. Khodasevych, L. Wang, A. Mitchell, and G. Rosengarten, “Micro- and nanostructured surfaces for selective solar absorption,” *Adv. Opt. Mater.* **3**, 852 (2015).
- ²⁴Y. Liu, H. Song, Z. Bei, L. Zhou, C. Zhao, B. S. Ooi, and Q. Gan, “Ultra-thin dark amorphous TiO_x hollow nanotubes for full spectrum solar energy harvesting and conversion,” *Nano Energy* **84**, 105872 (2021).
- ²⁵L. Zhou, Y. Tan, D. Ji, B. Zhu, P. Zhang, J. Xu, Q. Gan, Z. Yu, and J. Zhu, “Self-assembly of highly efficient, broadband plasmonic absorbers for solar steam generation,” *Sci. Adv.* **2**, e1501227 (2016).
- ²⁶S. A. Jalil, B. Lai, M. ElKabbash, J. Zhang, E. M. Garcell, S. Singh, and C. Guo, “Spectral absorption control of femtosecond laser-treated metals and application in solar-thermal devices,” *Light: Sci. Appl.* **9**, 14 (2020).
- ²⁷S. Fan and W. Li, “Photonics and thermodynamics concepts in radiative cooling,” *Nat. Photonics* **16**, 182 (2022).
- ²⁸L. Zhang, Z. Xu, L. Zhao, B. Bhatia, Y. Zhong, S. Gong, and E. N. Wang, “Passive, high-efficiency thermally-localized solar desalination,” *Energy Environ. Sci.* **14**, 1771 (2021).
- ²⁹N. Aubry, P. Singh, M. Janjua, and S. Nudurupati, “Micro- and nanoparticles self-assembly for virtually defect-free, adjustable monolayers,” *Proc. Natl. Acad. Sci. U. S. A.* **105**, 3711 (2008).
- ³⁰Fei Ding, “A review of multifunctional optical gap-surface plasmon metasurfaces,” *Prog. Electromagn. Res.* **174**, 55–73 (2022).
- ³¹N. Wu, Y. Zhang, H. Ma, H. Chen, and H. Qian, “Tunable High-Q plasmonic metasurface with multiple surface lattice resonances,” *Prog. Electromagn. Res.* **172**, 23–32 (2021).
- ³²B. Liu, J. Li, and S. Shen, “Resonant thermal infrared emitters in near- and far-fields,” *ACS Photonics* **4**, 1552 (2017).
- ³³J. Li, J. Wuenschell, Z. Li, S. Bera, K. Liu, R. Tang, H. Du, P. R. Ohodnicki, and S. Shen, “Fiber coupled near-field thermoplasmonic emission from gold nanorods at 1100 K,” *Small* **17**, 2007274 (2021).
- ³⁴R. Gardon, “A review of radiant heat transfer in glass,” *J. Am. Ceram. Soc.* **44**, 305 (1961).
- ³⁵J. A. Zasadzinski, R. Viswanathan, L. Madsen, J. Garnaes, and D. K. Schwartz, “Langmuir–Blodgett films,” *Science* **263**, 1726 (1994).
- ³⁶D. K. Lee, Y. H. Kim, C. W. Kim, H. G. Cha, and Y. S. Kang, “Vast magnetic monolayer film with surfactant-stabilized Fe₃O₄ nanoparticles using Langmuir–Blodgett technique,” *J. Phys. Chem. B* **111**, 9288 (2007).
- ³⁷D. Kraemer, B. Poudel, H.-P. Feng, J. C. Taylor, B. Yu, X. Yan, Y. Ma, X. Wang, D. Wang, A. Muto, K. McEnaney, M. Chiesa, Z. Ren, and G. Chen, “High-performance flat-panel solar thermoelectric generators with high thermal concentration,” *Nat. Mater.* **10**, 532 (2011).